

pubs.acs.org/biochemistry Article

# Catalytic Activity of the Archetype from Group 4 of the FTR-like Ferredoxin: Thioredoxin Reductase Family Is Regulated by Unique S = 7/2 and S = 1/2 [4Fe-4S] Clusters

Divya Prakash,\* Jin Xiong, Shikha S. Chauhan, Karim A. Walters, Hannah Kruse, Neela Yennawar, John H. Golbeck, Yisong Guo,\* and James G. Ferry\*



**Cite This:** *Biochemistry* 2024, 63, 1588–1598



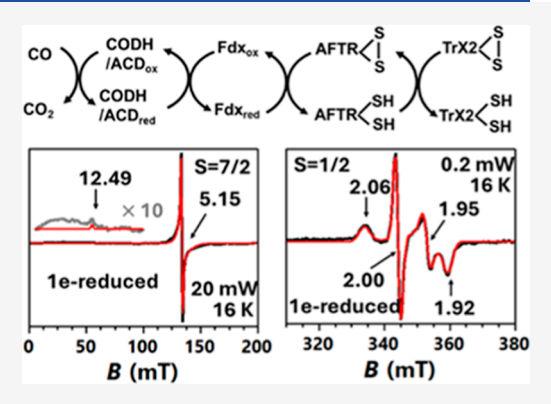
**ACCESS** I

III Metrics & More

Article Recommendations

Supporting Information

ABSTRACT: Thioredoxin reductases (TrxR) activate thioredoxins (Trx) that regulate the activity of diverse target proteins essential to prokaryotic and eukaryotic life. However, very little is understood of TrxR/Trx systems and redox control in methanogenic microbes from the domain Archaea (methanogens), for which genomes are abundant with annotations for ferredoxin:thioredoxin reductases [Fdx/thioredoxin reductase (FTR)] from group 4 of the widespread FTR-like family. Only two from the FTR-like family are characterized: the plant-type FTR from group 1 and FDR from group 6. Herein, the group 4 archetype (AFTR) from Methanosarcina acetivorans was characterized to advance understanding of the family and TrxR/Trx systems in methanogens. The modeled structure of AFTR, together with EPR and Mössbauer spectroscopies, supports a catalytic mechanism similar to plant-type FTR and FDR, albeit with important exceptions. EPR spectroscopy of reduced



AFTR identified a transient  $[4\text{Fe}-4\text{S}]^{1+}$  cluster exhibiting a mixture of S = 7/2 and typical S = 1/2 signals, although rare for proteins containing [4Fe-4S] clusters, it is most likely the on-pathway intermediate in the disulfide reduction. Furthermore, an active site histidine equivalent to residues essential for the activity of plant-type FTR and FDR was found dispensable for AFTR. Finally, a unique thioredoxin system was reconstituted from AFTR, ferredoxin, and Trx2 from M. acetivorans, for which specialized target proteins were identified that are essential for growth and other diverse metabolisms.

## **■ INTRODUCTION**

Thioredoxin systems are essential for the reduction of target proteins responsible for redox control of diverse metabolisms in all domains of life.<sup>1–3</sup> The systems are composed of an electron donor to thioredoxin reductase (TrxR) that reduces thioredoxin (Trx), which contains an invariant Cys-XX-Cys motif that forms a redox-active disulfide. Trx reduces the disulfide in target proteins by a dithiol—disulfide exchange mechanism.<sup>1–3</sup> Although uniformly distributed in all domains of life, very little is understood about TrxR/Trx systems in organisms from the domain *Archaea*, particularly methane producers (methanogens), the largest group of characterized species in the domain. Understanding redox control of methanogenesis is of ecological importance as biologically produced methane is a major greenhouse gas with a global warming potential approximately 20-fold greater than CO<sub>2</sub>.<sup>4</sup>

TrxRs are classified depending on the electron donor and active site configuration. TrxRs with FAD in the active site are dependent on NAD(P)H (NTR), coenzyme  $F_{420}$  ( $F_{420}$ ) (DFTR), or ferredoxin (Fdx) (FFTR) as the donor. The NAD(P)H-dependent TrxR enzymes have dominated investigations with only three Fdx-dependent enzymes described to date (FFTR, FTR, and FDR). Unlike FFTR, plant-type

Fdx:thioredoxin reductase (FTR) lacks FAD though it contains a unique [4Fe-4S] cluster and a redox-active cysteine disulfide in the active site. 10-12 Plant-type FTR is the founding member of a large family for which analyses of genome sequences reveal the family originated in deeply rooted microbes that later evolved structural diversification to meet the ecological requirements of diverse microbes from the domains *Bacteria* and *Archaea* (8). The family is composed of six groups of which the plant-type FTR belongs to group 1. FDR from *Methanosarcina acetivorans* belongs to group 6 and is the only other FTR-like family enzyme characterized so far. FDR reduces Trx5, one of seven Trx homologues identified in *M. acetivorans*. The crystal structure of FDR reveals an active site [4Fe-4S] cluster and a redox-active cysteine disulfide. Unlike FTR, FDR contains an additional domain that ligates a

Received: November 19, 2023 Revised: April 30, 2024 Accepted: May 21, 2024 Published: May 31, 2024





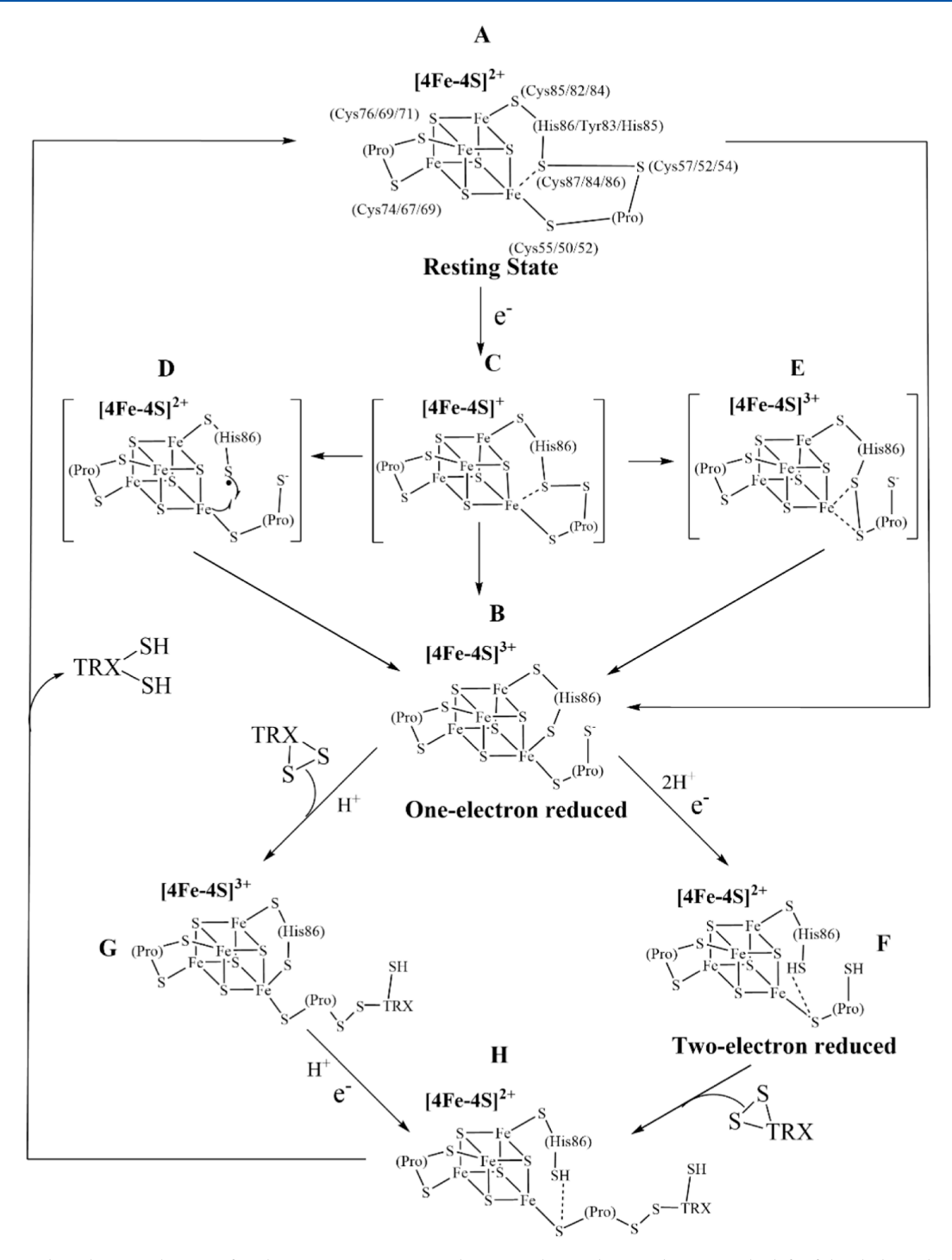


**Figure 1.** Proposed catalytic mechanisms for plant-type FTR, FDR, and AFTR. The residue numbering on the left of the slash mark is for FTR; the middle is for FDR, and to the right is for AFTR. Structures in parentheses are proposed one-electron-reduced intermediates.

[1Fe-0S] rubredoxin cluster proposed to transfer electrons from Fdx to the active site. A mechanism is proposed for FDR based on the structural, biochemical, and spectroscopic studies (Figure 1).

The mechanism involves reduction of the active-site disulfide (intermediate B, Figure 1), dependent on reduction of the resting state [4Fe-4S]<sup>2+</sup> cluster to [4Fe-4S]<sup>1+</sup> (intermediate C, Figure 1), which yields a unique one-electron-reduced [4Fe-4S]<sup>3+</sup> cluster containing a five-coordinate iron with two cysteine ligands. The penultimate step involves a second one-electron reduction to [4Fe-4S]<sup>2+</sup>

(intermediate H, Figure 1) and disulfide exchange with Trx by two possible mechanisms. A histidine in the active site of plant-type FTR plays an essential role in protonation/deprotonation of the cluster-interacting thiol, thereby anchoring it next to the cluster by forming an H-bond in the two-electron-reduced intermediate F (Figure 1).<sup>13</sup>

FDR shares the noncanonical CPC\*X<sub>n</sub>CPCX<sub>n</sub>CY/HC\* [4Fe-4S] motif of the FTR-like family for which the asterisked cysteines form the active-site disulfide. The remainder ligate the [4Fe-4S] cluster, in contrast to [4Fe-4S] clusters of diverse enzymes ligated with cysteines of the canonical

CX<sub>2</sub>CX<sub>2</sub>CX<sub>3</sub>CP motif. FDR intersects with the CoMS-SCoB heterodisulfide reductase (HDR) of methanogens by containing a noncanonical CX<sub>n</sub>CCX<sub>n</sub>CX<sub>2</sub>C [4Fe-4S] motif for which the cysteines ligate noncubane [4Fe-4S] clusters. 14 Similar to FDR and FTR, the proposed mechanism for HDR involves [4Fe-4S]3+ clusters with the S atoms of HSCoM or HSCoB ligated to a special five-coordinate Fe. 14 The only FTR-like family enzymes investigated are plant-type FTRs from group 1 and FDR from group 6, exposing a significant gap in understanding of the family. Here, we present a comprehensive analysis of AFTR (archaea-type FTR) found in M. acetivorans, the group 4 archetype. This analysis sheds light on the extensive FTR-like family and redox control in acetotrophic methanogens. Such methanogens are responsible for the majority of biologically produced atmospheric methane, a key contributor to the greenhouse effect and global warming. 15 Much is known about the biochemistry and molecular biology of the metabolic pathway converting acetate to methane but little about other factors controlling the process. Redox control of metabolism is of major importance in all domains of life, although it is neglected in acetotrophic methanogens for which catabolic pathways are highly regulated. The work reported here explores mechanisms of Fdx-dependent redox control in M. acetivorans, a model acetotrophic methanogen for which Fdx is the singular electron carrier essential for converting acetate to methane.

#### MATERIALS AND METHODS

**Materials.** *N*-Ethylmaleimide (NEM), cyanogen bromide-activated matrices, and bovine pancreas insulin were obtained from Sigma-Aldrich (St. Louis, MO, USA). DNA oligomers were obtained from Integrated DNA Technologies, Inc. (Coralville, IA, USA). The Q5 Site-Directed Mutagenesis Kit was purchased from New England Biolabs Inc. (Ipswich, MA, USA). The <sup>57</sup>Fe was purchased from *ISOFLEX* (San Francisco, CA, USA). DNA polymerase was purchased from Takara Bio Inc. (Mountain View, CA, USA). All other chemicals used were of analytical grade.

Cloning of AFTR (MA2870) and Trx2 (MA3212). The gene was amplified by PCR from genomic DNA using forward (<u>CATATG</u>ATGAGTGAACATGATGAATTAAAAAAT) and reverse (GTGCGGCCGC<u>AAGCTT</u>TCAGGAGGGCT TGAAGAAAA) primers with 15–17 bp extensions (bold) homologous to the pET-28a vector at NdeI (underlined) and *Hin*dIII (underlined) sites. The amplified gene was cloned into the NdeI and *Hin*dIII sites of the pET-28a vector (Novagen) using the In-Fusion (Clontech) cloning kit for expression with an *N*-terminal His<sub>6</sub> tag on AFTR. The AFTR-pET-28a (pMA2870) construct was validated by sequencing performed at the DNA Genomics Core Facility, Huck Institute of Life sciences, Penn State University. The Trx2-pEt22b(+) (pMA3212) construct used in this study is described elsewhere. <sup>16</sup>

Site-Directed Mutagenesis. The C86S, H85A, and H85Y variants of AFTR and the C21S variant of Trx2 were constructed using the Q5 Site-Directed Mutagenesis Kit from New England Biolabs Inc. (Ipswich, MA, USA). In brief, mutations were introduced by directly amplifying the expression vectors (pMA2870 and pMA3212) containing the AFTR and Trx2 genes, respectively, using the primers shown in Table S4. The PCR products obtained after amplification were incubated with Kinase-Ligase-DpnI (KLD) enzyme mix for 10 min at 21 °C and transferred into 5-alpha competent

Escherichia coli (New England Biolabs) for ligation of the linearized vector. The correct plasmids were validated by sequencing performed at the DNA Genomics Core Facility, Huck Institute of Life Sciences, Penn State University.

**Protein Expression and Purification.** AFTR and its variants (C86S, H85A, and H85A) were overexpressed and anaerobically purified by adapting the protocol used for FDR.<sup>7</sup> Wild-type Trx2 and the C21S variant were heterologously produced and purified as described elsewhere.<sup>16</sup> The CO dehydrogenase/decarbonylase (CODH/ACD) complex and Fdx were purified from *M. acetivorans* by adapting protocols described elsewhere.<sup>17</sup> NEM modification of wild-type AFTR was performed as reported elsewhere.<sup>7,18</sup> See Supporting Information for details.

Insulin Disulfide Reductase Activity of Trx2 Dependent on Reduced Wild-Type AFTR and Variants. AFTR and variants were reduced with dithionite (DT), which was found incapable of reducing Trx2 and insulin. The assay mixture (0.8 mL) contained 150 mM NaCl, 0.13 mM insulin, 6  $\mu$ M Trx2, and 5  $\mu$ M of either wild-type AFTR, H85Y variant, or the H85A variant in 50 mM phosphate buffer (pH 6.5). The reaction was initiated by the addition of 5 mM sodium DT and performed at 21 °C in an anaerobic chamber (Cov Manufacturing). The time course of Trx2-dependent reduction of insulin was monitored turbidimetrically at 650 nm as described by Holmgren.<sup>19</sup> The activity was expressed as the ratio of the slope of a linear part of the turbidity curve to the lag time (reported as  $\Delta A_{650}/\text{min} \times 10^{-3}/\text{mg}$ ), as described previously. 20,21 No measurable activity was detected in the absence of insulin, Trx2, or wild-type AFTR and variants.

**Identification of AFTR and Trx2 Target Proteins.** The methods were adapted from those previously reported for thioredoxin target proteins in plants and *bacteria*. See Supporting Information for details.

**EPR Spectroscopy.** CW EPR studies were carried out at the X-band (9.64 GHz) using a Bruker E500 spectrometer and a cylindrical TE 011 mode resonator (Bruker BioSpin Corp, Billerica, MA). An ESR-910 liquid helium cryostat and ITC-4 controller (Oxford Instruments) maintained the temperature at 15 K. Determination of EPR signal intensities was carried out by measuring the individual S = 1/2 species under nonsaturating conditions. As the signals represent the first derivative of the absorption signal, the spectra were double integrated and the area of each signal was compared with that of a 10 mM copper-sulfate standard (10 mM CuSO<sub>4</sub>, 2 M NaClO<sub>4</sub>, and 10 mM HCl). The values obtained this way were compared to the known enzyme concentration, which was set to 80% of the [4Fe-4S] clusters in dimeric AFTR. Only the intensities of the [4Fe-4S]<sup>1+</sup> in wild type and [4Fe-4S]<sup>3+</sup> in NEM-modified wild type (NEM-AFTR) could be determined as described. The amount of EPR silent S = 0 resting-state [4Fe-4S]<sup>2+</sup> was assigned as the difference between the concentration of AFTR present and the concentration of paramagnetic species. The detailed CW X-band EPR studies of the  $S = 7/2 [4\text{Fe}-4\text{S}]^{1+}$  state in wild-type AFTR and [4Fe-4S]3+ in wild-type NEM-AFTR were carried out by using a Bruker E500A spectrometer equipped with a Bruker ER4116DM dual mode cavity and an Oxford ESR910 cryostat for low temperature measurement. The sample temperature was calibrated using a mimic sample, a calibrated carbon-glass resistor (Lakeshore CGR-1-1000) placed in an EPR tube. The spin quantification was relative to that of a 1.20 mM Cu(II)-EDTA standard. The spectral simulations were performed on

the SpinCount software with a conventional spin Hamiltonian as below <sup>25</sup>

$$\hat{H} = D\left(\hat{S}_{zz}^2 - \frac{S(S+1)}{3}\right) + E(\hat{S}_{xx}^2 - \hat{S}_{yy}^2) + \beta \hat{\mathbf{S}} \cdot \mathbf{g} \cdot \hat{\mathbf{B}}$$

where

$$D = \frac{3}{2}D_{zz}, \ E = \frac{1}{2}(D_{xx} - D_{yy}), \ |D_{zz}| \ge |D_{yy}| \ge |D_{xx}|$$

Mössbauer Spectroscopy. Mössbauer spectra were recorded on constant acceleration Mössbauer spectrometers equipped with either a Janis SVT-400 variable-temperature cryostat (weak-field) or a Janis 8T MOSS-OM-12SVT variable-temperature cryostat (strong-field). Isomer shifts are reported with respect to the centroid of the spectrum of the α-iron metal at room temperature. Simulations of Mössbauer spectra were carried out by the program WMOSS (Seeco, Edina, MN) and Spincount (Prof. Michael P. Hendrich, CMU, PA). Calculations invoking the spin Hamiltonian formalism were performed according to the equation listed below, in which the former term describes the interaction between the electric field gradient and the nuclear quadrupole moment, and the latter term represents the nuclear Zeeman splitting of  $^{57}$ Fe nuclei. All symbols have their usual meaning.  $^{26,27}$ 

$$\begin{split} \hat{H} &= \sum_{i} \left\{ \frac{eQV_{zz,i}}{4 \mathbb{I}_{i}(2\mathbb{I}_{i}-1)} [3\widehat{I_{z,i}}^{2} - I_{i}(I_{i}+1) + \eta_{i}(\widehat{I_{x,i}}^{2} - \widehat{I_{y,i}}^{2})] - g_{n}\beta_{n}\widehat{I_{i}} - \hat{B} \right\}, \\ where &\ \eta_{i} = \frac{V_{xx,i} - V_{yy,i}}{V_{xx,i}}, \ |V_{xx,i}| \leq |V_{yy,i}| \leq |V_{zz,i}| \end{split}$$

## RESULTS

Bioinformatics. A BLAST search of nonredundant databases with the query AFTR (MA2870) (https://blast.ncbi. nlm.nih.gov/Blast.cgi) retrieved homologues from diverse species in the domains Bacteria and Archaea. The first 100 sequences had >83% sequence coverage and >52% identity, for which representatives are shown in Figure S1. The large majority belongs to methanogens from the domain Archaea indicating that AFTR plays a collective role in this group. The sequences showed the C-terminal domain of FDR absent, and the active site Tyr83 of FDR replaced with His85 in AFTR, for which the cognate His of plant FTR is essential.<sup>13</sup> In addition, multiple sequence alignment reveals the presence of another conserved His residue (H74) in the AFTR homologue with a currently unknown function.<sup>13</sup> Although the noncanonical [4Fe-4S] motif of FDR and plant FTR is conserved in AFTR, the overall sequence identities between AFTR and FDR or AFTR and plant FTR were no greater than 32% (Figure S2). These analyses show that AFTR belongs to group 4 of the FTR-like family replete with AFTR homologues from diverse methanogens.8

Structure and Biochemistry. The *N*-terminal His<sub>6</sub>-tagged wild type and variants (H85Y, H85A, H74Y, and C86S) of AFTR were produced in *E. coli* strain Δ*iscR* and anaerobically purified to electrophoretic homogeneity. SDS/PAGE of the wild type and variants (Figure S3) indicated monomer molecular masses of 11 kDa consistent with the calculated value of 10 kDa. Size-exclusion chromatography of the wild type and variants estimated native molecular masses of approximately 20 kDa (data not shown), which indicated homodimers in solution. Solvent envelope structures determined by homology modeling and biological small-angle X-ray

scattering (BioSAXS) (Table S1 and Figures S4–10, and more description of BioSAXS results in the Supporting Information) superposed well for both AFTR and FDR as dimers.

Notably, AFTR lacks the C-terminal domain of FDR that ligates a [1Fe-0S] rubredoxin-like cluster. However, homology modeling of AFTR showed similarity to that of the active site in the *N*-terminal domain of FDR. Figure 2A,B shows the

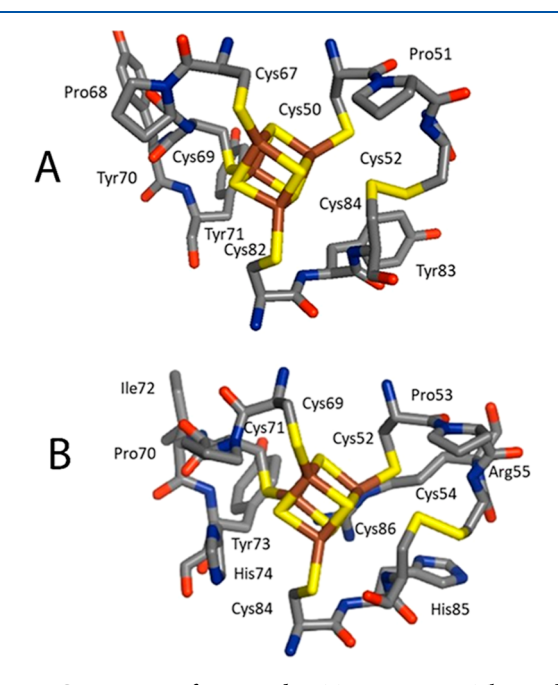
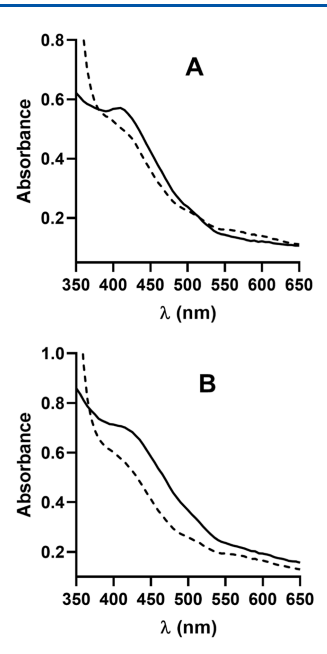


**Figure 2.** Comparison of FDR and AFTR active sites. The model of AFTR was obtained using AlphaFold.<sup>28</sup> The active sites of FDR (A) and AFTR (B) contain the [4Fe-4S] cluster and active-site disulfides. Atoms are color coded for iron (brown), sulfur (yellow), carbon (gray), nitrogen (blue), and oxygen (red).

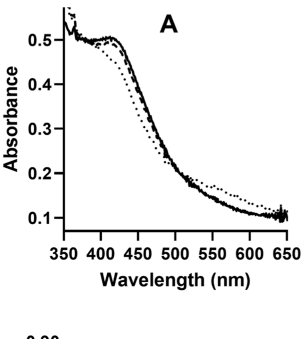
solvent-exposed disulfides formed by the cluster-interacting thiols of AFTR C86 and FDR C84 and the interchange thiols of AFTR C54 and FDR C52 in the proximity of the respective [4Fe-4S] clusters. The comparison also shows H85 of AFTR in the equivalent position of Y83 of FDR.

The wild type, H85Y variant, H85A variant, H74Y variant, and C86S variant contained 7.3  $\pm$  0.6 (n = 3), 6.9  $\pm$  0.8 (n = 3), 7.6  $\pm$  0.5 (n = 3), 6.7  $\pm$  0.8 (n = 3), and 7.5  $\pm$  0.4 (n = 3) iron and 7.8  $\pm$  0.4(n = 3), 7.1  $\pm$  0.6 (n = 3), 6.8  $\pm$  0.7 (n = 3), 7.7  $\pm$  0.3 (n = 3), and 7.1  $\pm$  0.8 (n = 3) sulfur per dimer. The wild type, H85A variant, and C86S variant purified from *E. coli* cultured with  $^{57}$ Fe contained 5.9  $\pm$  0.8 (n = 3), 7.2  $\pm$  0.3, and 6.8  $\pm$  0.7 (n = 3) iron per dimer. The results are consistent with one [4Fe–4S] cluster per monomer as predicted from sequence analysis (Figure S2). The UV–visible spectrum of the as-purified wild type showed a broad absorbance band with an  $\lambda_{\rm max}$  of 412 nm that was bleached by the addition of DT indicating reduction of the [4Fe–4S]²+ cluster (Figure 3A).

Fdx is required for all methanogenic pathways and is the exclusive electron carrier in acetotrophic species that account for most of the methane produced in Earth's biosphere. Central to all acetotrophic pathways is the CO dehydrogenase/acetyl-CoA decarbonylase (CODH/ACD) complex for which Fdx is the electron acceptor. Figures 4 and S12 show that Fdx isolated from acetate-grown *M. acetivorans* mediates electron transfer from the CODH/ACD to AFTR, which



**Figure 3.** Spectral changes accompanying reduction of as-purified wild-type AFTR and wild-type NEM-AFTR. (A) Wild type  $(34 \mu M)$  and (B) wild-type NEM-AFTR  $(43 \mu M)$ . Key: (-) air-oxidized, (--) recorded 1.0 min after addition of 0.3 mM (final concentration) sodium DT.



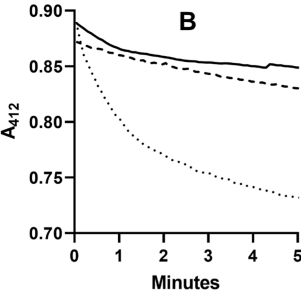


Figure 4. Fdx-dependent reduction of wild-type AFTR. The complete reaction mixture (700  $\mu$ L) contained CODH/ACD (26  $\mu$ g or 0.12  $\mu$ M considering the molecular weight of CODH complex is 297 kDa based on as reported for CODH complex from *M. thermophila*<sup>31</sup>), AFTR (45  $\mu$ M), Fdx (28  $\mu$ g or 6.4  $\mu$ M), and NaCl (150 mM) in 50 mM phosphate buffer (pH 7.4). The anaerobic reactions were contained in a serum-stoppered cuvette (2 mL) with 1 atm of CO and initiated by the addition of CODH/ACD. Panel A, UV–vis spectra. Key: (–) complete mixture minus CODH/ACD and Fdx, (-- -) complete mixture at time zero, and (···) complete mixture after 5 min incubation. Panel B, time course for reduction monitored at 412 nm. Key: (–) complete mixture minus CODH, (-- -) complete mixture minus Fdx, and (···) complete mixture containing AFTR/CODH/Fdx.

shows that AFTR is Fdx-dependent and is the archetype of group 4 in the FTR-like family.

AFTR Target Proteins. A method for detecting AFTR target proteins was developed based on the mechanism proposed for FDR (Figure 1) in which target proteins form a mixed disulfide intermediate with the interchange thiol of C54. The intermediate is stabilized when AFTR lacks the cluster interacting thiol of C86 (Figure 1, structure H), which attacks the mixed disulfide, releasing the reduced target protein (Figure 1). The method is analogous to that developed for chloroplast Trx utilizing the active site serine variant, which stabilizes the mixed disulfides containing target proteins that are released from Trx by reduction with dithiothreitol (DTT).<sup>23</sup> The AFTR C86S variant was immobilized on a CNBr-activated Sepharose column, to which was applied an air-oxidized crude protein preparation from M. acetivorans grown with acetate. Proteomic analysis of the DTT-eluted fraction identified 178 proteins (Table S2), which included Trx2, previously shown to reduce the disulfide of insulin with

Figure 5 shows the reduction of Trx2 dependent on AFTR and Fdx reduced with CODH/ACD. The results support an in

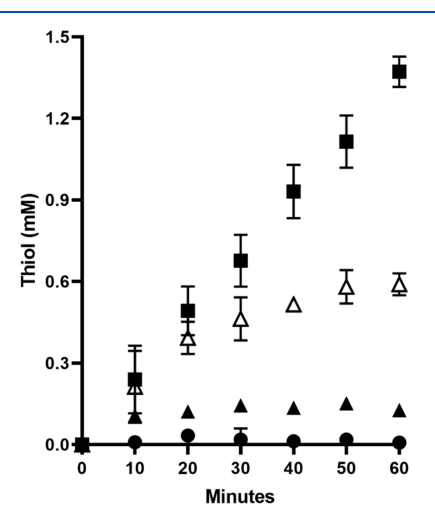
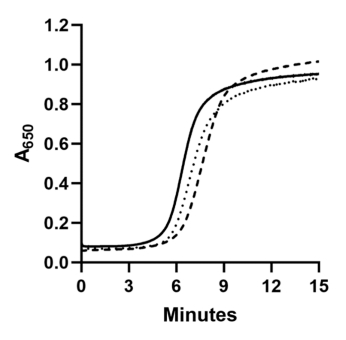


Figure 5. Fdx-dependent disulfide reductase activity of wild-type AFTR. The complete reaction mixture (400  $\mu$ L) contained 20  $\mu$ g of CODH/ACD, 8.6  $\mu$ M Fdx, 7  $\mu$ M wild-type AFTR, 12.5  $\mu$ M Trx2, and 400  $\mu$ g of insulin in 50 mM phosphate buffer (pH 7.4). The reaction mixture was contained in a serum-stoppered vial (2.0 mL) with 1.0 atm CO. The reactions were started by adding CODH/ACD. Reduction of insulin and Trx2 was monitored with Ellman's reagent detecting the formation of thiols. Reaction mixtures: ( $\blacksquare$ ) complete, ( $\blacksquare$ ) minus Fdx, ( $\Delta$ ) minus insulin, and ( $\Delta$ ) minus Trx2. Thiol levels detected for reactions minus AFTR or minus AFTR and insulin (not shown) were not significantly different from the reaction mixture minus Fdx. Data points and bars are the mean and standard deviation of three experiments.

vivo role for an Fdx/AFTR/Trx2 thioredoxin system. Figure S11 shows the energy minimized complex derived from modeled structures of AFTR, Fdx, and Trx2.

Furthermore, the insulin disulfide reductase (IDS) activity of Trx2 was determined with DT-reduced AFTR (Figure 6).

The IDS measures the turbidity at 650 nm, which has been shown to be used before to test the activity of other thioredoxin-like proteins. <sup>20,32,33</sup> The AFTR/Trx2 system with DT as an electron source was exploited further to determine the role for H85 of AFTR in the reduction of Trx2. The rate of



**Figure 6.** Insulin disulfide reductase activity of Trx2 reduced with wild-type AFTR or H85Y/A variants. The reaction mixture contains 6  $\mu$ M AFTR (solid line), H85Y-AFTR (dashed line), H85A-AFTR (dotted line), 50  $\mu$ g of Trx2, and 1 mg of insulin. The reaction was started by adding DT (1.8 mM). No increase in absorbance at 650 nm was observed in the following control reactions: (i) DT, insulin, and Trx2; (ii) DT, insulin, and AFTR; (iii)/(iv), DT, insulin, and H85Y/H85A.

insulin reduction ( $\Delta A_{650}$  min<sup>-2</sup> x  $10^{-3}$ /mg) by Trx2, reduced with wild-type AFTR, was  $49.8 \pm 3.2$  compared to  $47.2 \pm 3.8$  and  $44.9 \pm 5.7$  for the H85Y and H85A variants. Thus, the variants show comparable activity to that of wild type in Trx2 reduction to wild type. This result contrasts with that reported for the equivalent H86Y variant of plant FTR, which only exhibited 10% activity of the wild-type FTR<sup>7,13</sup>—a result that further distinguishes AFTR from FTR. Based on this observation, it has been suggested that H86 of FTR may serve as the key proton source for disulfide reduction. However, in AFTR, H85 seems to be dispensable for the disulfide reduction activity, and it may use another residue to fulfill the proton transfer role in the enzymatic reaction. As indicated in the bioinformatics section, H74 is identified as

another conserved residue in AFTR homologues, which is close to the [4Fe-4S] cluster based on structural homologue modeling and may function as the proton source (Figure 2). Thus, we tested the activity of the AFTR H74Y variant. However, the activity of AFTR H74Y is almost equal to that of WT AFTR (Figure S13), therefore ruling out a significant functional role for H74 in AFTR. Further studies are needed to identify the key proton source for AFTR activity. Nevertheless, these observations further distinguish AFTR from FTR.

**Trx2 Target Proteins.** The finding that Trx2 eluted from the affinity column and was reduced by AFTR presented the possibility that Trx2 formed a stable mixed disulfide with the C86S variant of AFTR and bound air-oxidized proteins in the cell-free extract. Protein targets of Trx2 were identified utilizing a C21S variant of Trx2, which eliminates the thiol attacking the mixed disulfide, thereby stabilizing the intermediate for release of bound proteins by DTT analogous to that described for chloroplast Trx.<sup>24</sup> The variant was immobilized on a CNBractivated Sepharose column, to which was applied the airoxidized crude protein extract from acetate-grown M. acetivorans. Proteomic analysis of the DTT-eluted fraction identified 187 proteins (Table S2), of which 110 matched AFTR targets. A control experiment in the absence of the AFTR C86S variant or Trx2 C21S variant yielded only one protein encoded by the MA3387 locus with the annotation of an uncharacterized protein. These results indicate that AFTR plays roles in diverse processes either directly or in the Fdx/ AFTR/Trx2 system.

**Mechanism.** The active site of AFTR was investigated by Mössbauer and EPR spectroscopies to advance the understanding of the unique iron—sulfur cluster in AFTR.

The low-field-low-temperature Mössbauer spectra (Figure 7A,B) of the as-purified and DT-reduced AFTR exhibited a

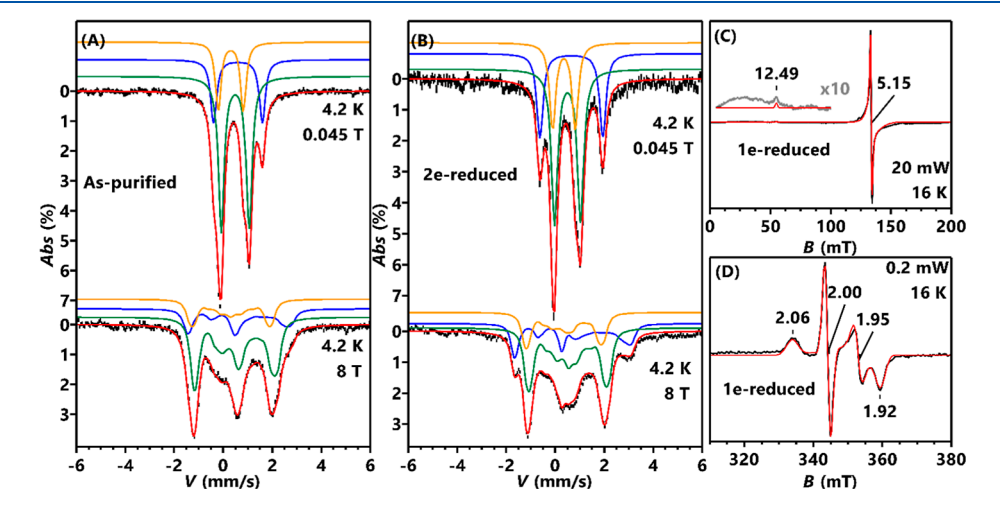


Figure 7. Spectroscopy of the [4Fe4S] cluster in as-purified, one-electron-reduced, and two-electron-reduced wild-type AFTR. Panels A and B. Mössbauer spectra of 0.778 mM <sup>57</sup>Fe AFTR proteins as purified (A) and after incubation with 20 equiv of DT for 30 min (B) showing [4Fe4S]<sup>2+</sup> cluster signals. Black lines represent experimental spectra and the associated statistical error; red lines show total spectral simulations; simulations of the subcomponents are color coded: green, mixed-valent Fe<sup>2+</sup>Fe<sup>3+</sup> pair; blue, valence localized Fe<sup>2+</sup> site; yellow, valence localized Fe<sup>3+</sup> site. Panels C and D. X-band cw-EPR spectra of reduced wild-type AFTR in the presence of MV show the S = 7/2 species (C) and the S = 1/2 species (D). The EPR sample was prepared by mixing 0.2 mM of WT-AFTR with 0.1 equiv of MV and 10 equiv of DT and incubating the solution for 80 s before freezing it for EPR analysis. Black and red lines show the experimental data and the spectral simulations, respectively. The inset in Panel C contains the scaled (10x) spectral signal and the simulation showing the weak resonance at g = 12.49. Sample information and measurement conditions are indicated in the Figure. For Mössbauer spectra, the external field is parallel to the γ-radiation. Mössbauer simulation parameters are listed in Table 1. EPR simulation parameters: for the S = 7/2 species, g = [2.03, 2.01, 2.09], D = -1.45 cm<sup>-1</sup>, E/D = 0.116,  $\sigma(E/D) = 0.012$ , concentration = 0.017 mM; for the S = 1/2 cluster, S = 1/2 cluster

quadrupole-doublet feature reflecting three different iron sites assigned to a valence localized Fe<sup>2+</sup>, a valence localized Fe<sup>3+</sup>, and a pair of valence delocalized Fe<sup>2+</sup>/Fe<sup>3+</sup> with an intensity ratio of ~1:1:2. The isomer shift ( $\delta$ ) and quadrupole splitting ( $\Delta E_{\rm Q}$ ) values are typical of [4Fe–4S]<sup>2+</sup> clusters similar to those reported for FDR and plant FTR<sup>-,31,34</sup> (Table 1).

Table 1. Mössbauer Parameters of Various Forms of Wild-Type AFTR and Variants

sample	site	$\delta$ mm/s	$\frac{\Delta E_{\mathrm{O}}}{\mathrm{mm/s}}$	$\eta^d$	area (%)	note
wild type	I	0.61	1.99	0.3	23	Fe <sup>2+</sup>
	II	0.48	1.14	0.5	55	$\mathrm{Fe^{2+}/Fe^{3+}}$
	III	0.31	1.04	1.0	23	Fe <sup>3+</sup>
reduced wild type <sup>a</sup>	Ι	0.66	2.56	0.1	25	Fe <sup>2+</sup>
	II	0.51	1.05	0.8	46	$\mathrm{Fe^{2+}/Fe^{3+}}$
	III	0.36	0.92	0.7	25	Fe <sup>3+</sup>
H85A variant	I	0.55	1.89		23	Fe <sup>2+</sup>
	II	0.49	1.13		55	$\mathrm{Fe^{2+}/Fe^{3+}}$
	III	0.28	1.08		23	Fe <sup>3+</sup>
reduced H85A variant <sup>b</sup>	Ι	0.68	2.50		22	Fe <sup>2+</sup>
	II	0.51	1.09		44	$\mathrm{Fe^{2+}/Fe^{3+}}$
	III	0.34	0.96		22	Fe <sup>3+</sup>
	$IV^c$	0.55	1.89		3	Fe <sup>2+</sup>
	$V^c$	0.49	1.13		7	$\mathrm{Fe^{2+}/Fe^{3+}}$
	$VI^c$	0.28	1.08		3	Fe <sup>3+</sup>

<sup>a</sup>As-purified <sup>57</sup>Fe wild-type AFTR incubated with excess sodium DT for 30 min. <sup>b</sup>As-purified <sup>57</sup>Fe H85A variant incubated with excess sodium DT for 5 min. <sup>c</sup>Site IV, V, and VI are corresponding to the resting state. <sup>d</sup>The asymmetry parameter,  $\eta$ , was determined by the 8-T Mössbauer spectra.

The spin state of the cluster in both as-purified and reduced AFTR was confirmed to be diamagnetic (S = 0) by the spectral data measured under the high field condition (Figure 7A,B). The Mössbauer spectra and parameters of as-purified and reduced AFTR are similar to those reported for FDR and FTR. Therefore, as-purified AFTR and the reduced AFTR can be assigned to the resting state (structure A, Figure 1) and the two-electron-reduced state, respectively (structure F, Figure 1).

The proposed mechanism of FDR includes a transient  $[4Fe-4S]^{3+}$  intermediate after one-electron reduction of the as-purified enzyme (structure B, Figure 1) that can be stabilized on selective alkylation of the reactive C52 thiol by N-ethylmaleimide (NEM). $^{7,13,34}$  The NEM modified aspurified wild-type AFTR (NEM-AFTR) showed pronounced optical features at 425 nm that shifted to 410 nm after reduction (Figure 3B), a result characteristic of the  $[4Fe-4S]^{3+}$  cluster observed for NEM-FDR and NEM-modified plant FTR (NEM-FTR). $^{7,11}$  This result was confirmed by EPR measurements, showing a near-axial EPR signal with g = [2.12, 2.0, 1.98], typical of a  $[4Fe-4S]^{3+}$  cluster (Figure S14).

The mechanism shown in Figure 1 also involves a transient one-electron-reduced intermediate (structures D, C, or E).  $^{7,11}$  In FDR, a typical Fdx-like S=1/2 [4Fe-4S]  $^{1+}$  cluster is observed by EPR for this intermediate. In AFTR, the use of methyl viologen (MV) as a redox mediator during the reduction of AFTR allowed a higher accumulation of all EPR signals (Figure 6B,C). The rhombic signal with g=[2.06, 1.95, 1.92] and the isotropic signal at g=2 are typical of Fdx-like S=1/2 [4Fe-4S]  $^{1+}$  clusters and a MV radical, respectively (Figure

7D). Additional EPR resonances at g = 12.49 and 5.15 were also observed, which have not been observed in reduced FDR<sup>7,11</sup> (Figure 7C). Careful EPR analysis (Figure S15, see the Supporting Information for details) revealed that these resonances for AFTR are from an S = 7/2 spin state with the g = 12.49 resonance originating from the  $m_s = \pm 1/2$  Kramers' doublet and the g = 5.15 resonance originating from the  $m_s =$ ± 3/2 doublet. Temperature-dependent measurements revealed that this S = 7/2 species exhibits a small negative zero field splitting parameter ( $D = -1.45 \text{ cm}^{-1}$ ) and a relatively large rhombicity (E/D = 0.12) (Figure S13, Table S3). Upon longer incubation with DT, such as 5 min, the signal intensities of both S = 1/2 and S = 7/2 species decreased and almost disappeared (Figure S16). This result, along with the observation of a single [4Fe-4S]<sup>2+</sup> cluster in the Mössbauer spectra of the two-electron-reduced AFTR, led us to assign the S = 7/2 species to a  $[4Fe-4S]^{1+}$  cluster, which coexists with an S = 1/2  $[4Fe-4S]^{1+}$  cluster in reduced AFTR. Both types of  $[4Fe-4S]^{1+}$  clusters are assigned to intermediate C in the reaction mechanism (Figure 1). These results establish conversion of the [4Fe-4S]1+ cluster intermediate (structure C, Figure 1) to the two-electron-reduced intermediate (structure F, Figure 1) as reported for FDR.

## DISCUSSION

**Mechanism.** The mechanism proposed for AFTR is similar to that proposed for FDR and plant FTR (Figure 1), albeit with important differences.<sup>7,-,34</sup> Like FDR and FTR, it is proposed that resting-state AFTR (structure A) contains a unique Fe in the  $[4Fe-4S]^{2+}$  cluster that weakly interacts with the active-site disulfide  $(C_{54}-S-S-C_{86})$ , as shown by Mössbauer data. Supported by spectroscopic data of NEM-AFTR, a one-electron-reduced intermediate (structure B, Figure 1) is proposed in which the disulfide is cleaved and the cluster-interacting thiol of C86 ligates to the unique Fe site to yield the  $S = 1/2 [4Fe-4S]^{3+}$  cluster. This intermediate accepts another electron, yielding the two-electron-reduced intermediate (structure F, Figure 1) confirmed by Mössbauer. The two-electron-reduced enzyme revealed an S = 0 [4Fe-4S]2+ cluster with more pronounced perturbation of the unique Fe site compared with those in the resting state revealed by the change of its Mössbauer parameters (Table 1), rationalized by strong interaction with cluster-interacting C86 observed previously for FDR and FTR.7 In the two-electronreduced intermediate, the strong interaction of the unique Fe site with C86 is conceivably the consequence of a strong Hbond between the thiol of cluster interacting C86 and the S atom of C52 that leaves the interchangeable thiol of C54 free to attack substrates. The presence of free interchangeable thiol C54 on both the one-electron (structure B) and two-electronreduced intermediate (structure F) makes intermediates B and F capable of carrying out an attack on the Trx2 substrate to generate the Trx2-bound AFTR intermediate H (Figure 1). In the final step, the thiolate of C86 is proposed to attack the heterodisulfide bridge of structure H, releasing reduced Trx2 and reforming the active-site disulfide (C<sub>54</sub>-S-S-C<sub>86</sub>) of resting-state structure A.

Although the mechanism proposed for AFTR resembles that for FTR and FDR, novel features were also observed. EPR spectroscopy of reduced AFTR identified a transient one-electron-reduced  $[4\text{Fe}-4\text{S}]^{1+}$  cluster that exhibits a mixture of the S=7/2 and S=1/2 signals attributed to structure C (Figure 1). To our knowledge, S=7/2 species has not been

observed in FTR-like domain-containing proteins, although it has been reported for proteins with iron-sulfur clusters substituted with selenium [4Fe-4Se]<sup>35,36</sup> and the [4Fe-4S] cluster in the benzoyl-CoA reductase from Thauera aromatica.<sup>37</sup> Theoretically, different ground spin states of a cluster are the consequence of different cluster core geometry distortions, which lead to different spin coupling schemes. In a typical [4Fe-4S]<sup>1+</sup> cluster with a  $D_{2d}$  symmetry (an E distortion from the parent  $T_d$  symmetry),<sup>38</sup> the pair of the high spin (S=2)  $Fe^{2+}$  atoms are ferromagnetically coupled to form an s=4state, which is antiferromagnetically coupled to the valence delocalized  $Fe^{2+}Fe^{3+}$  pair with s = 9/2 to yield a total ground spin state of S = 1/2. An S = 7/2 ground state possibly comes from a  $T_2$  distortion (from the parent  $T_d$  symmetry) of the cluster core.<sup>38</sup> Such a distortion creates C<sub>3</sub> symmetry with three equivalent iron sites and one unique iron site. For a [4Fe-4S]<sup>1+</sup> cluster, it is anticipated that the Fe<sup>3+</sup> center could be the unique site, which possibly exhibits strong antiferromagnetic exchange interactions with the other three equivalent Fe2+ centers, which in turn forces the spins of the three equivalent Fe2+ centers to align (provided that the exchange interactions among the three Fe<sup>2+</sup> centers are much weaker). Thus, an S = 7/2 state can be stabilized by the coupling scheme where three  $S = 2 \text{ Fe}^{2+}$  ions are ferromagnetically coupled to form an S = 6 state, which then antiferromagnetically couple to the unique  $S = 5/2 \text{ Fe}^{3+}$ . A similar spin coupling scheme has been successfully used to explain an S = 4 all ferrous [4Fe-4S]<sup>0</sup> cluster where an apical Fe<sup>2+</sup> (on the C3 axis) antiferromagnetically couples to three ferromagnetically coupled Fe<sup>2</sup> atoms. <sup>38</sup> Alternatively, direct cluster core modifications could also lead to the stabilization of a S = 7/2 state. For example, Suess and co-workers recently reported a synthetic S = 7/2 [4Fe-4S] cluster with a novel alkylation on one of the bridging sulfides.<sup>39</sup> Such a structural modification would weaken the exchange couplings among the three iron centers ligated by this alkylated sulfide, thus leading to the aforementioned magnetic coupling scheme to stabilize the S =7/2 state. Thus, the observation of the S = 7/2 species indicates that the geometry of the [4Fe-4S]1+ in AFTR is most likely distorted (or modified) differently from that of a conventional S = 1/2 cluster. The crystal structure of AFTR, along with spectroscopic analysis of other active-site variants, is warranted to elucidate the formation of this novel S = 7/2species in AFTR.

Nevertheless, the S = 7/2 [4Fe-4S]<sup>1+</sup> in AFTR (together with the S = 1/2 [4Fe-4S]<sup>1+</sup>) is most likely the key reactive intermediate in the disulfide reduction activity not only because a long-time incubation of AFTR with DT fully convert the [4Fe-4S]<sup>1+</sup> state to the two-electron-reduced state (Figures 7 and S16) but also because the S = 7/2 intermediate is also formed during catalytic turnover in the presence of Trx2, the substrate of AFTR. Specifically, an identical S = 7/2 species is observed in the EPR analysis of a sample containing AFTR, Trx2, and insulin that is reduced by DT (the reaction mixture to detect AFTR-mediated insulin disulfide reductase activity) (Figure S17).

Another unique feature of AFTR is residue H85 positioned equivalent to Y83 in FDR and H86 in plant FTR (Figures 1 and 2). The histidine is conserved in all but one of the AFTR homologues found in microbes from the domains *Bacteria* and *Archaea* (Figure S1). Residue H86 of plant-type FTR is essential for activity and proposed to protonate C87, promoting an H-bond between the thiol of C87 and the S

atom of C55 that stabilizes substrate binding to the twoelectron-reduced intermediate (structure F, Figure 1). The two-electron-reduced intermediate is not formed in the H86Y variant of plant FTR. 18 Residue H85 of AFTR is ligated to C86 of the active-site disulfide  $(C_{54}-S-S-C_{86})$  like ligation of H86 to C87 of the plant FTR active site disulfide  $(C_{57}-S-S-C_{87})$ (Figures 1 and 2). However, activities of the H85Y and H85A variants of AFTR were found near equal to that of wild-type AFTR in contrast to near complete loss of activity reported for the H86Y variant of plant FTR. 40 The Y83H variant of FDR is reported to have twice the enzymatic activity of the wild type, indicating that histidine can replace tyrosine. However, near equal activity of wild type and the H85A/Y variant indicates a nonessential role for H85 in AFTR. The nonessential role of H85 was supported further by the ability of H85A to form the two-electron-reduced intermediate like that observed in wildtype AFTR (Figure S18, Table 1) unlike plant FTR. 13 Possibly, other residues or a solvent molecule provides a pathway for protonation of C86 in AFTR to facilitate binding of the substrate to the two-electron-reduced intermediate F (Figure 1).

**Physiology.** The results extend a physiological role for Fdx-dependent FrxR/Trx systems beyond that first described in plants. As Fdx is the singular electron carrier in acetotrophic methanogens, establishment of the Fdx/AFTR/Trx2 system in *M. acetivorans* advances understanding of redox control of metabolic processes responsible for most of the methane produced in Earth's biosphere that contributes to the greenhouse effect and global warming.

A role for the Fdx/AFTR/Trx2 system in redox control of diverse metabolic processes in M. acetivorans is supported by the finding that an abundance of proteins of diverse function are potential targets of either AFTR or both AFTR and Trx2. Notably, the glutaredoxin system of redox control is absent in most methanogens, including M. acetivorans, which implicates a dependence on TrxR/Trx systems.<sup>2,42-44</sup> Notably, the CODH/ACD complex is central to the pathway of methanogenesis from acetate and a target of the Fdx/AFTR/Trx2 system among enzymes essential to the pathway (Table S2). The complex requires strong reducing conditions consistent with a role for the system in reactivation or redox regulation of the pathway analogous to Fdx-dependent redox control of carbon flow in plants.<sup>45</sup> The Fdx reduced in photosystem I donates electrons to FTR, which reduces chloroplast Trx, in turn regulating enzyme activities by reduction, which regulates carbon flow.4

The capability of M. acetivorans to adapt and grow in the presence of permanent low  $O_2$  levels and sustain viability when exposed to  $H_2O_2$  suggests it mounts a substantial defense against oxidative stress. <sup>47,48</sup> Indeed, peroxiredoxin and rubrerythrin are among the target proteins identified with the potential for redox control by the Fdx/AFTR/Trx2 system.

### CONCLUSIONS

The present findings advance an understanding of the FTR-like family of TrxRs by characterizing AFTR, the group 4 archetype with homologues widely distributed in the domains *Bacteria* and *Archaea*, although dominant in methanogens. Reconstitution of the Fdx/AFTR/Trx2 system has contributed to physiological understanding of redox control in acetotrophic methanogens responsible for most methane produced in Earth's biosphere. Identification of target proteins has provided a foundation for continued investigation of the system.

Furthermore, a catalytic mechanism is supported for AFTR that involves a one-electron-reduced  $[4Fe-4S]^{1+}$  intermediate previously hypothesized for FDR and FTR. EPR spectroscopy of the intermediate identified a mixture of a novel S=7/2 signal and a typical S=1/2 signal. This observation is unique for enzymes containing [4Fe-4S] clusters. Finally, the results show a histidine in AFTR is not essential for activity, although cognate to the histidine is essential to stabilize substrate binding in FTR.

#### ASSOCIATED CONTENT

#### **Data Availability Statement**

All relevant data are in this manuscript and its Supporting Information files.

## Supporting Information

The Supporting Information is available free of charge at https://pubs.acs.org/doi/10.1021/acs.biochem.3c00651.

Results on EPR simulation of the  $S = 7/2 [4Fe-4S]^{1+}$ ; experimental procedures (details on proteins expression and purification, insulin disulfide reductase activity, identification of AFTR and TrX2 targets, and BioSAXS modeling); sequence alignments of AFTR from M. acetivorans with homologues; multiple sequence alignment of FDR, AFTR, and FTR; SDS-PAGE of purified proteins; solution structure and active-site region of AFTR compared with the structure of FDR; SAXS raw data collected anaerobically for AFTR; Guinier plot for the AFTR SAXS data; Kratky plots derived from AFTR SAXS data; pair distance distribution function p(r)obtained from the AFTR SAXS data; dimer model of AFTR; conserved interface of the AFTR dimer; energy minimized complex of a monomer of AFTR with Fdx and Trx2; Fdx-dependent reduction of wild-type AFTR; insulin disulfide reductase activity of Trx2 reduced with wild-type AFTR or H74Y variant; X-band cw-EPR spectra of air-exposed AFTR-NEM complexes; X-band cw-EPR spectra of sodium DT-reduced wild-type AFTR in the presence of 0.1 equiv of MV; time course of change in the [4Fe-4S]<sup>1+</sup> EPR signal intensity of DTreduced resting-state wild-type AFTR; EPR spectroscopic evidence of the formation of the S = 7/2 species in the reaction mixture with the presence of Trx2 and insulin; Mössbauer spectroscopic evidence of the [4Fe-4S] cluster in as-purified and two-electron-reduced wildtype AFTR and the H85A variant; SAXS structural parameters of AFTR; proteomic identification of proteins acquired from cell-free extracts by immobilized AFTR or Trx2; EPR simulation parameters for reduced AFTR; and primers used for amplification of genes and the construction of plasmids (PDF)

### **Accession Codes**

Archaeal Ferredoxin Thioredoxin Reductase (AFTR): MA2870. Thioredoxin 2 (Trx2): MA3212

## AUTHOR INFORMATION

### **Corresponding Authors**

Divya Prakash — School of Chemical and Biomolecular Sciences, Southern Illinois University-Carbondale, Carbondale, Illinois 62901, United States; oorcid.org/ 0000-0003-0080-2583; Email: divya.prakash@siu.edu

**Yisong Guo** – Department of Chemistry, The Carnegie Mellon University, Pittsburgh, Pennsylvania 15213, United States;

orcid.org/0000-0002-4132-3565; Email: ysguo@andrew.cmu.edu

James G. Ferry – Department of Biochemistry and Molecular Biology, The Pennsylvania State University, University Park, Pennsylvania 16802, United States; Email: jgf3@psu.edu

#### Authors

Jin Xiong — Department of Chemistry, The Carnegie Mellon University, Pittsburgh,, Pennsylvania 15213, United States; orcid.org/0000-0001-7443-0554

Shikha S. Chauhan – School of Chemical and Biomolecular Sciences, Southern Illinois University-Carbondale, Carbondale, Illinois 62901, United States

Karim A. Walters – Department of Biochemistry and Molecular Biology, The Pennsylvania State University, University Park, Pennsylvania 16802, United States

Hannah Kruse – School of Chemical and Biomolecular Sciences, Southern Illinois University-Carbondale, Carbondale, Illinois 62901, United States

Neela Yennawar — The Huck Institutes of the Life Sciences, The Pennsylvania State University, University Park, Pennsylvania 16802, United States; occid.org/0000-0001-7278-659X

John H. Golbeck – Department of Chemistry, The Pennsylvania State University, University Park, Pennsylvania 16802, United States; Department of Biochemistry and Molecular Biology, The Pennsylvania State University, University Park, Pennsylvania 16802, United States

Complete contact information is available at: https://pubs.acs.org/10.1021/acs.biochem.3c00651

## **Author Contributions**

JGF, DP, JX, SSC, and YG conceived the study. SSC, DP, KAW, JX, HK, and NY performed the experiments. JGF, YG, DP, JX, JHG, and NY wrote the manuscript. JX and DP contributed equally. All authors analyzed the results and approved the final version of the manuscript.

#### **Funding**

This work was supported by the Division of Chemical Sciences, Geosciences, and Biosciences, Office of Basic Energy Sciences of the U.S. Department of Energy through grant DE-FG02—95ER20198 to JGF and DP; DE-SC0018087 to JHG and the Person endowment to JGF. DP thanks for the support of the Energy Boost Seed Grant from Advanced Energy Institute and Illinois Soybean Center, Southern Illinois University, Carbondale. YG thanks for the funding support from the National Institutes of Health under award number #R01-GM125924. Research reported on BioSAXS was supported by SIG S10 of the National Institutes of Health under award number #S10-OD028589-01 to NY.

#### Notes

The authors declare no competing financial interest.

# ACKNOWLEDGMENTS

The authors thank Dr. Tatiana Laremore at the Penn State Proteomics and Mass Spectrometry Core Facility for the acquisition of proteomics data and manuscript preparation.

## REFERENCES

(1) Jacquot, J. P.; Eklund, H.; Rouhier, N.; Schürmann, P. Structural and evolutionary aspects of thioredoxin reductases in photosynthetic organisms. *Trends Plant Sci.* **2009**, *14*, 336–343.

- (2) Meyer, Y.; Buchanan, B. B.; Vignols, F.; Reichheld, J. P. Thioredoxins and glutaredoxins: unifying elements in redox biology. *Annu. Rev. Genet.* **2009**, *43*, 335–367.
- (3) Lu, J.; Holmgren, A. The thioredoxin antioxidant system. Free Radical Biol. Med. 2014, 66, 75–87.
- (4) Ramaswamy, V.; Boucher, O.; Haigh, J.; Hauglustaine, D.; Haywood, J.; Myhre, G.; Nakajima, T.; Shi, G. Y.; Solomon, S. Radiative forcing of climate change, In Climate Change 2001: The Scientific Basis. Contribution of Working Group I to the Third Assessment Report of the Intergovernmental Panel on Climate Change; Houghton, J. T.; Ding, Y.; Griggs, D. J.; Noguer, M.; van der Linden, P. J.; Dai, X.; Maskell, K.; Johnson, C. A., Eds.: Cambridge University Press, Cambridge, U. K, 2001; pp 349–416,
- (5) McCarver, A. C.; Lessner, F. H.; Soroeta, J. M.; Lessner, D. J. Methanosarcina acetivorans utilizes a single NADPH-dependent thioredoxin system and contains additional thioredoxin homologues with distinct functions. *Microbiology* **2017**, *163*, 62–74.
- (6) Susanti, D.; Loganathan, U.; Mukhopadhyay, B. A novel F<sub>420</sub>-dependent thioredoxin reductase gated by low potential FAD: a tool for redox regulation in an anaerobe. *J. Biol. Chem.* **2016**, *291*, 23084–23100.
- (7) Prakash, D.; Walters, K. A.; Martinie, R. J.; McCarver, A. C.; Kumar, A. K.; Lessner, D. J.; Krebs, C.; Golbeck, J. H.; Ferry, J. G. Towards a mechanistic and physiological understanding of a ferredoxin:disulfide reductase from the domains *Archaea* and *Bacteria*. *J. Biol. Chem.* **2018**, 293, 9198–9209.
- (8) Balsera, M.; Uberegui, E.; Susanti, D.; Schmitz, R. A.; Mukhopadhyay, B.; Schurmann, P.; Buchanan, B. B. Ferredoxin:thioredoxin reductase (FTR) links the regulation of oxygenic photosynthesis to deeply rooted bacteria. *Planta* **2013**, 237, 619–635.
- (9) Buey, R. M.; Fernandez-Justel, D.; de Pereda, J. M.; Revuelta, J. L.; Schurmann, P.; Buchanan, B. B.; Balsera, M. Ferredoxin-linked flavoenzyme defines a family of pyridine nucleotide-independent thioredoxin reductases. *Proc. Natl. Acad. Sci. U.S.A.* **2018**, *115*, 12967—12972.
- (10) Dai, S.; Friemann, R.; Glauser, D. A.; Bourquin, F.; Manieri, W.; Schürmann, P.; Eklund, H. Structural snapshots along the reaction pathway of ferredoxin-thioredoxin reductase. *Nature* **2007**, 448, 92–96.
- (11) Walters, E. M.; Johnson, M. K. Ferredoxin:thioredoxin reductase: disulfide reduction catalyzed *via* novel site-specific [4Fe-4S] cluster chemistry. *Photosynth. Res.* **2004**, *79*, 249–264.
- (12) Jameson, G. N.; Walters, E. M.; Manieri, W.; Schürmann, P.; Johnson, M. K.; Huynh, B. H. Spectroscopic evidence for site specific chemistry at a unique iron site of the [4Fe-4S] cluster in ferredoxin:thioredoxin reductase. *J. Am. Chem. Soc.* **2003**, 125, 1146–1147.
- (13) Walters, E. M.; Garcia-Serres, R.; Naik, S. G.; Bourquin, F.; Glauser, D. A.; Schürmann, P.; Huynh, B. H.; Johnson, M. K. Role of histidine-86 in the catalytic mechanism of ferredoxin:thioredoxin reductase. *Biochemistry* **2009**, *48*, 1016–1024.
- (14) Wagner, T.; Koch, J.; Ermler, U.; Shima, S. Methanogenic heterodisulfide reductase (HdrABC-MvhAGD) uses two noncubane [4Fe-4S] clusters for reduction. *Science* **2017**, *357*, 699–703.
- (15) Ferry, J. G. Methanosarcina acetivorans: a model for mechanistic understanding of aceticlastic and reverse methanogenesis. *Front. Microbiol.* **2020**, *11*, 1806.
- (16) Kumar, A. K.; Kumar, R. S.; Yennawar, N. H.; Yennawar, H.; Ferry, J. G. Structural and biochemical characterization of a ferredoxin:thioredoxin reductase-like enzyme from *Methanosarcina acetivorans*. *Biochemistry* **2015**, *54*, 3122–3128.
- (17) Yan, Z.; Wang, M.; Ferry, J. G. A Ferredoxin- and  $F_{420}H_2$ -dependent, electron-bifurcating, heterodisulfide reductase with homologs in the domains *Bacteria* and *Archaea. mBio* **2017**, 8, No. e02285.
- (18) Walters, E. M.; Garcia-Serres, R.; Jameson, G. N.; Glauser, D. A.; Bourquin, F.; Manieri, W.; Schürmann, P.; Johnson, M. K.; Huynh, B. H. Spectroscopic characterization of site-specific [Fe4S4]

- cluster chemistry in ferredoxin: thioredoxin reductase: implications for the catalytic mechanism. *J. Am. Chem. Soc.* **2005**, *127*, 9612–9624.
- (19) Holmgren, A. Thioredoxin catalyzes the reduction of insulin disulfides by dithiothreitol and dihydrolipoamide. *J. Biol. Chem.* **1979**, 254, 9627–9632.
- (20) Martinez-Galisteo, E.; Padilla, C.; Garcia-Alfonso, C.; Lopez-Barea, J.; Barcena, J. Purification and properties of bovine thioredoxin system. *Biochimie* **1993**, *75*, 803–809.
- (21) Shi, Y.-y.; Tang, W.; Hao, S.-f.; Wang, C.-C. Contributions of cysteine residues in Zn2 to zinc fingers and thiol-disulfide oxidoreductase activities of chaperone DnaJ. *Biochemistry* **2005**, *44*, 1683–1689.
- (22) Susanti, D.; Wong, J. H.; Vensel, W. H.; Loganathan, U.; Desantis, R.; Schmitz, R. A.; Balsera, M.; Buchanan, B. B.; Mukhopadhyay, B. Thioredoxin targets fundamental processes in a methane-producing archaeon, *Methanocaldococcus jannaschii*. *Proc. Natl. Acad. Sci. U.S.A.* **2014**, *111*, 2608–2613.
- (23) Motohashi, K.; Romano, P. G.; Hisabori, T. Identification of Thioredoxin Targeted Proteins Using Thioredoxin Single-Cysteine Mutant-Immobilized Resin. In *Plant Signal Transduction*; Springer, 2009; pp 117–131.
- (24) Motohashi, K.; Kondoh, A.; Stumpp, M. T.; Hisabori, T. Comprehensive survey of proteins targeted by chloroplast thioredoxin. *Proc. Natl. Acad. Sci. U.S.A.* **2001**, *98*, 11224–11229.
- (25) Petasis, D. T.; Hendrich, M. P. Quantitative interpretation of multifrequency multimode EPR spectra of metal containing proteins, enzymes, and biomimetic complexes. *Methods Enzymol.* **2015**, *563*, 171–208.
- (26) Münck, E. Aspects of <sup>57</sup>Fe Mössbauer Spectroscopy; University Science Books, Sausalito, CA, 2000.
- (27) Pandelia, M. E.; Lanz, N. D.; Booker, S. J.; Krebs, C. Müssbauer spectroscopy of Fe/S proteins. *Biochim. Biophys. Acta* **2015**, *1853*, 1395–1405.
- (28) Jumper, J.; Evans, R.; Pritzel, A.; Green, T.; Figurnov, M.; Ronneberger, O.; Tunyasuvunakool, K.; Bates, R.; Zidek, A.; Potapenko, A.; Bridgland, A.; Meyer, C.; Kohl, S. A. A.; Ballard, A. J.; Cowie, A.; Romera-Paredes, B.; Nikolov, S.; Jain, R.; Adler, J.; Back, T.; Petersen, S.; Reiman, D.; Clancy, E.; Zielinski, M.; Steinegger, M.; Pacholska, M.; Berghammer, T.; Bodenstein, S.; Silver, D.; Vinyals, O.; Senior, A. W.; Kavukcuoglu, K.; Kohli, P.; Hassabis, D. Highly accurate protein structure prediction with AlphaFold. *Nature* 2021, 596, 583–589.
- (29) Welte, C.; Deppenmeier, U. Bioenergetics and anaerobic respiratory chains of aceticlastic methanogens. *Biochim. Biophys. Acta* **2014**, *1837*, 1130–1147. 11
- (30) Wang, M.; Tomb, J. F.; Ferry, J. G. Electron transport in acetate-grown *Methanosarcina acetivorans*. *BMC Microbiol.* **2011**, *11*, 165.
- (31) Abbanat, D. R.; Ferry, J. G. Resolution of component proteins in an enzyme complex from *Methanosarcina thermophila* catalyzing the synthesis or cleavage of acetyl-CoA. *Proc. Natl. Acad. Sci. U.S.A.* **1991**, 88, 3272–3276.
- (32) McCarver, A. C.; Lessner, D. J. Molecular characterization of the thioredoxin system from *Methanosarcina acetivorans*. FEBS J. **2014**, 281, 4598–4611.
- (33) Yenugudhati, D.; Prakash, D.; Kumar, A. K.; Kumar, R. S.; Yennawar, N. H.; Yennawar, H. P.; Ferry, J. G. Structural and biochemical characterization of methanoredoxin from *Methanosarcina acetivorans*, a glutaredoxin-like enzyme with coenzyme M-dependent protein disulfide reductase activity. *Biochemistry* 2015, 55, 313–321.
- (34) Staples, C. R.; Gaymard, E.; Stritt-Etter, A. L.; Telser, J.; Hoffman, B. M.; Schürmann, P.; Knaff, D. B.; Johnson, M. K. Role of the  $[\operatorname{Fe}_4S_4]$  cluster in mediating disulfide reduction in spinach ferredoxin:thioredoxin reductase. *Biochemistry* **1998**, *37*, 4612–4620.
- (35) Jung, Y.-S.; Vassiliev, I. R.; Golbeck, J. H. Crossover of a high-spin ( $S=7/2,\,3/2$ ) to a low-spin (S=1/2) iron-selenium cluster in FA and FB of photosystem I on rebinding of PsaC onto P700-FX cores. *JBIC, J. Biol. Inorg. Chem.* **1997**, *2*, 209–217.

- (36) Moulis, J. M.; Auric, P.; Gaillard, J.; Meyer, J. Unusual features in EPR and Mossbauer spectra of the 2[4Fe-4Se]<sup>+</sup> ferredoxin from *Clostridium pasteurianum. J. Biol. Chem.* **1984**, 259, 11396–11402.
- (37) Boll, M.; Albracht, S. S. P.; Fuchs, G. Benzoyl-CoA reductase (dearomatizing), a key enzyme of anaerobic aromatic metabolism: A study of adenosinetriphosphatase activity, ATP stoichiometry of the reaction and EPR properties of the enzyme. *Eur. J. Biochem.* 1997, 244, 840–851.
- (38) Chakrabarti, M.; Deng, L.; Holm, R. H.; Munck, E.; Bominaar, E. L. Mossbauer, electron paramagnetic resonance, and theoretical studies of a carbene-based all-ferrous Fe4S4 cluster: electronic origin and structural identification of the unique spectroscopic site. *Inorg. Chem.* **2009**, *48*, 2735–2747.
- (39) Ye, M.; Brown, A. C.; Suess, D. L. Reversible alkyl-group migration between iron and sulfur in [Fe4S4] clusters. *J. Am. Chem. Soc.* **2022**, *144*, 13184–13195.
- (40) Glauser, D. A.; Bourquin, F.; Manieri, W.; Schürmann, P. Characterization of ferredoxin:thioredoxin reductase modified by site-directed mutagenesis. *J. Biol. Chem.* **2004**, *279*, 16662–16669.
- (41) Balmer, Y.; Vensel, W. H.; Cai, N.; Manieri, W.; Schurmann, P.; Hurkman, W. J.; Buchanan, B. B. A complete ferredoxin/thioredoxin system regulates fundamental processes in amyloplasts. *Proc. Natl. Acad. Sci. U.S.A.* **2006**, *103*, 2988–2993.
- (42) Fahey, R. C. Glutathione analogs in prokaryotes. *Biochim. Biophys. Acta* 2013, 1830, 3182–3198.
- (43) McFarlan, S. C.; Terrell, C. A.; Hogenkamp, H. P. C. The purification, characterization, and primary structure of a small redox protein from *Methanobacterium thermoautotrophicum*, an archaebacterium. *J. Biol. Chem.* **1992**, *267*, 10561–10569.
- (44) Ondarza, R. N.; Rendon, J. L.; Ondarza, M. Glutathione reductase in evolution. J. Mol. Evol. 1983, 19, 371-375.
- (45) Bhaskar, B.; DeMoll, E.; Grahame, D. A. Redox-dependent acetyl transfer partial reaction of the acetyl-CoA decarbonylase/synthase complex: kinetics and mechanism. *Biochemistry* **1998**, *37*, 14491–14499.
- (46) Schürmann, P. Redox signaling in the chloroplast: the ferredoxin/thioredoxin system. *Antioxid. Redox Signal.* **2003**, *5*, 69–78
- (47) Jasso-Chavez, R.; Santiago-Martinez, M. G.; Lira-Silva, E.; Pineda, E.; Zepeda-Rodriguez, A.; Belmont-Diaz, J.; Encalada, R.; Saavedra, E.; Moreno-Sanchez, R. Air-adapted *Methanosarcina acetivorans* shows high methane production and develops resistance against oxygen stress. *PLoS One* **2015**, *10*, No. e0117331.
- (48) Horne, A. J.; Lessner, D. J. Assessment of the oxidant tolerance of *Methanosarcina acetivorans*. *FEMS Microbiol*. *Lett.* **2013**, 343, 13–19.